

---

This is an electronic reprint of the original article.  
This reprint may differ from the original in pagination and typographic detail.

Kukkola, Jarno; Hinkkanen, Marko

## State observer for grid-voltage sensorless control of a grid-connected converter equipped with an LCL filter

*Published in:*

The 16th European Conference on Power Electronics and Applications (EPE'14 ECCE Europe)

*DOI:*

[10.1109/EPE.2014.6910740](https://doi.org/10.1109/EPE.2014.6910740)

Published: 26/08/2014

*Document Version*

Peer-reviewed accepted author manuscript, also known as Final accepted manuscript or Post-print

*Please cite the original version:*

Kukkola, J., & Hinkkanen, M. (2014). State observer for grid-voltage sensorless control of a grid-connected converter equipped with an LCL filter. In *The 16th European Conference on Power Electronics and Applications (EPE'14 ECCE Europe)* <https://doi.org/10.1109/EPE.2014.6910740>

---

This material is protected by copyright and other intellectual property rights, and duplication or sale of all or part of any of the repository collections is not permitted, except that material may be duplicated by you for your research use or educational purposes in electronic or print form. You must obtain permission for any other use. Electronic or print copies may not be offered, whether for sale or otherwise to anyone who is not an authorised user.

# State Observer for Grid-Voltage Sensorless Control of a Grid-Connected Converter Equipped With an LCL Filter

Jarno Kukkola and Marko Hinkkanen  
Aalto University School of Electrical Engineering  
Department of Electrical Engineering and Automation  
P.O. Box 13000, FI-00076 Aalto  
Espoo, Finland  
E-mail: jarno.kukkola@aalto.fi, marko.hinkkanen@aalto.fi

## Acknowledgments

The authors would like to thank ABB Oy, Walter Ahlström Foundation, and Finnish Foundation for Technology Promotion for the financial support.

## Keywords

«Adaptive observer», «grid-connected converter», «grid-voltage sensorless», «sensorless control», «small-signal linearization»

## Abstract

This paper proposes a simple grid-voltage sensorless alternative to the conventional PLL synchronization for a grid-connected converter equipped with an LCL filter. The grid-voltage magnitude and angle are estimated based only on the converter current and DC-voltage measurements. Reduced number of sensors decreases costs and amount of sensor wiring. The analytically derived design is validated experimentally.

## 1. Introduction

Three-phase grid converters equipped with an AC-side LCL filter are increasingly used to connect various renewable and distributed energy sources as well as motor drives to the electric grid. Interest for using LCL filters has increased, because they afford better grid-current quality, lower cost, and smaller physical size in comparison with the L filter. The control scheme of these converters is usually implemented in the grid-voltage or grid-flux synchronous reference frame (dq), in the natural reference frame (abc), or in the stationary reference frame ( $\alpha\beta$ ). Regardless of the reference frame, synchronization with the grid is needed for instantaneous active and reactive power control. Conventionally, synchronization is achieved using some variant of the phase-locked loop (PLL) to detect the angle of the measured grid voltage. If the grid voltage is not measured, the synchronization can be based on: 1) control error ( $i_{c,ref} - i_c$ ) of current control [1]; 2) DC-link power balance [2]; 3) instantaneous power theory [3]; 4) duality between the grid-connected converter and the PWM inverter-fed electric motor [4, 5]; 5) direct estimation [6, 7]; or 6) adaptive model-based estimation [8]. The above-mentioned methods have been developed for a grid-connected converter using the conventional L filter, but in the case of the resonant LCL filter, only a few [9–13] grid-voltage sensorless synchronization methods exist.

For the grid-voltage sensorless synchronization in the case of the LCL filter, the Kalman filter has been used to directly detect the grid voltage together with LCL filter states [9]. Instead of direct estimation, in [10], the grid voltage has been adapted using the grid-current estimation error of the Kalman filter. However, the process noise parameters for the Kalman filter, which determine the dynamics of the observer, have to be determined by trial and error [9]. In [11], power-theory-based grid-voltage estimation

has been proposed for the converter with an LCL filter, but instead of the grid voltage, the capacitor voltage of the LCL filter has been estimated. In the case of the grid converter equipped with an LC filter, a neural-network grid-voltage estimator has been presented in [14], and a steepest-descent adaptation algorithm has been used for the grid-voltage estimation. Moreover, the series resistance and inductance have been identified in parallel with the grid-voltage estimator in [14]. The parallel estimators provide the self-tuning feature, but high expertise of modern control theory is needed when designing and analyzing the neural-network estimator. Similar algorithms have been used without neural networks [12], whereupon the additional value of neural networks with these relatively simple models can be challenged. Furthermore, in the case of LCL filters, the steepest-descent algorithm has been used with the adaptive observers [12, 13] to directly estimate the grid voltage from the converter current estimation error of the Kalman filter [12], or to give an estimate of the aggregated uncertainties, which include information about the grid voltage [13].

In this paper, an estimation method for the grid-voltage magnitude and angle is proposed. The proposed method is based on the full-order observer [15], which is augmented with adaptation loops for the grid voltage magnitude and angle. Only the AC-side converter currents and the DC-side voltage are measured. In the adaptation loops, grid-voltage estimation is based on regulating the error between the measured and estimated converter currents to zero using proportional-integral (PI) controllers. Grid-voltage and state estimation reduce the number of sensors, which provides cost advantages and decreases the amount of sensor wiring. Analytical design rules, enabling automatic tuning of the estimation method, are also proposed. First, the system model and the observer are defined. Then, adaptation loops are formulated and their dynamics are analyzed by means of small-signal linearization. The expressions for the observer and adaptation gains are given as functions of system parameters and desired dynamics. Finally, simulation and experimental results are presented.

## 2. Model

The equivalent circuit model of the LCL filter model, between converter and grid, is presented in Fig. 1. The grid voltage in the stationary reference frame is

$$\mathbf{u}_g^s = e^{j\vartheta_g} u_g, \quad (1)$$

where  $\vartheta_g = \int \omega_g dt$  is the angle,  $\omega_g$  is the angular frequency, and  $u_g$  is the amplitude of the grid voltage. When the converter-side current  $i_c$ , the capacitor voltage  $u_f$ , and the grid-side current  $i_g$  of the LCL filter are selected as state variables, the LCL filter dynamics in a reference frame rotating at the angular frequency of  $\hat{\omega}_g$  are

$$\frac{d}{dt} \underbrace{\begin{bmatrix} i_c \\ u_f \\ i_g \end{bmatrix}}_{\mathbf{x}} = \underbrace{\begin{bmatrix} -j\hat{\omega}_g & -\frac{1}{L_{fc}} & 0 \\ \frac{1}{C_f} & -j\hat{\omega}_g & -\frac{1}{C_f} \\ 0 & \frac{1}{L_{fg}} & -j\hat{\omega}_g \end{bmatrix}}_{\mathbf{A}} \begin{bmatrix} i_c \\ u_f \\ i_g \end{bmatrix} + \underbrace{\begin{bmatrix} \frac{1}{L_{fc}} \\ 0 \\ 0 \end{bmatrix}}_{\mathbf{B}_c} \mathbf{u}_c + \underbrace{\begin{bmatrix} 0 \\ 0 \\ -\frac{1}{L_{fg}} \end{bmatrix}}_{\mathbf{B}_g} \mathbf{u}_g, \quad \mathbf{i}_c = \underbrace{\begin{bmatrix} 1 & 0 & 0 \end{bmatrix}}_{\mathbf{C}_c} \mathbf{x}, \quad (2)$$

where  $\mathbf{u}_c$  and  $\mathbf{u}_g$  are the converter and grid voltages, respectively, and  $L_{fc}$ ,  $C_f$ , and  $L_{fg}$  are the LCL filter parameters. The losses of the filter are neglected, which represents the worst-case situation for the

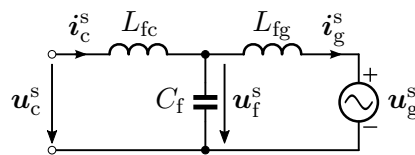


Fig. 1: The grid-connected LCL filter. The superscript  $s$  refers to the stationary reference frame, which is used for the sake of simplicity.

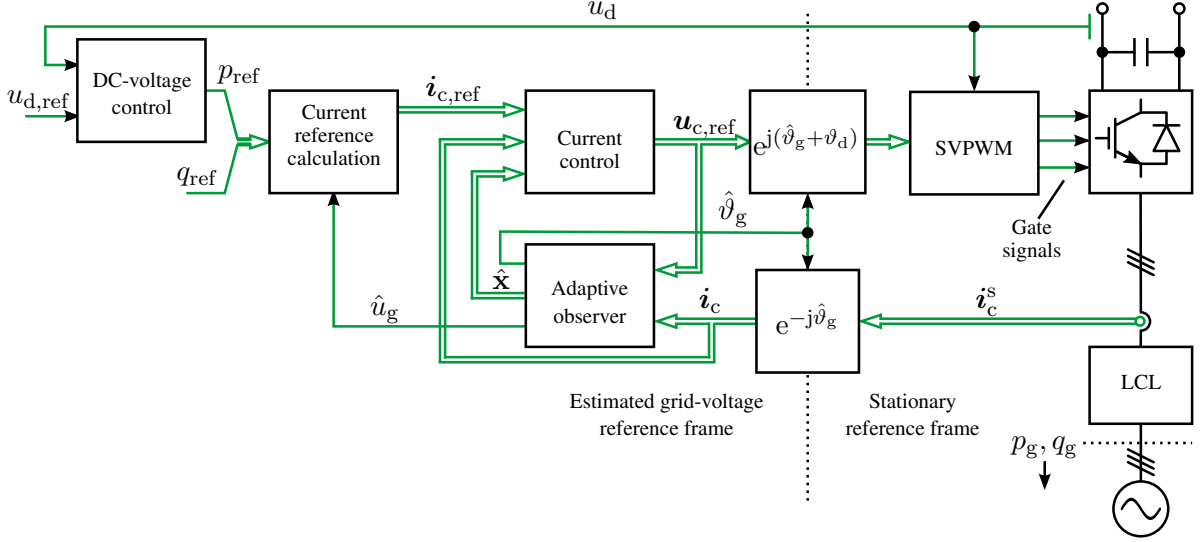


Fig. 2: Block diagram of the control system.

resonance of the LCL filter. Switching-cycle-averaged complex-valued space vectors are used (e.g., the converter current  $\mathbf{i}_c = i_{cd} + j i_{cq}$ ). Complex, matrix, and vector quantities are marked with boldface symbols.

### 3. Adaptive Observer

The block diagram of the control system is shown in Fig. 2. The power balance is regulated with a DC-voltage controller together with an inner state-space current controller [15]. The full-order observer estimates the state variables  $\mathbf{x} = [i_c \ \mathbf{u}_f \ i_g]^T$  for the state-space controller. The observer gain vector  $\mathbf{L} = [l_1 \ l_2 \ l_3]^T$  can be expressed by desired dynamic behavior and system parameters, as in [15], contrary to the Kalman filter whereby the knowledge of the noise covariances is needed [9, 12]. The synchronous reference frame of the control system is tied to the estimated grid voltage, i.e.,  $\hat{\mathbf{u}}_g = \hat{u}_g + j0$ , and it is rotating at estimated grid-voltage angular frequency of  $\hat{\omega}_g$ . The magnitude and angle of the grid voltage are estimated using an adaptation loop, explained later.

In the selected reference frame, the full-order observer is

$$\dot{\hat{\mathbf{x}}} = \hat{\mathbf{A}}\hat{\mathbf{x}} + \hat{\mathbf{B}}_c \mathbf{u}_c + \hat{\mathbf{B}}_g \hat{\mathbf{u}}_g + \mathbf{L}(\mathbf{i}_c - \hat{\mathbf{i}}_c), \quad \hat{\mathbf{i}}_c = \mathbf{C}_c \hat{\mathbf{x}}, \quad (3)$$

where the estimated quantities are marked with  $\hat{\cdot}$ , and  $\hat{\mathbf{A}}$ ,  $\hat{\mathbf{B}}_c$  and  $\hat{\mathbf{B}}_g$  consist of nominal (estimated) system parameters  $\hat{L}_{fc}$ ,  $\hat{C}_f$ , and  $\hat{L}_{fg}$ . If accurate circuit parameters are assumed, i.e.,  $\hat{\mathbf{B}}_c = \mathbf{B}_c$ ,  $\hat{\mathbf{B}}_g = \mathbf{B}_g$ , and  $\hat{\mathbf{A}} = \mathbf{A}$ , the dynamics of the estimation error  $\mathbf{e} = \mathbf{x} - \hat{\mathbf{x}}$  are obtained from (2) and (3) as

$$\dot{\mathbf{e}} = (\mathbf{A} - \mathbf{L}\mathbf{C}_c)\mathbf{e} + \mathbf{B}_g(e^{j(\vartheta_g - \hat{\vartheta}_g)} \mathbf{u}_g - \hat{\mathbf{u}}_g), \quad (4)$$

where  $\hat{\vartheta}_g$  is estimated angle of the grid voltage. As can be seen from the equation, the estimation error dynamics are nonlinear and are affected by the angle difference  $\vartheta_g - \hat{\vartheta}_g$  between the reference frames of the grid voltage and the observer and the difference  $u_g - \hat{u}_g$  between the grid-voltage magnitude and its estimate. In the following, the error dynamics are linearized in order to examine these relationships more closely.

#### 3.1. Linearization

The nonlinear dynamics of (4) can be linearized using small-signal approach. The operation point quantities are marked by subscript 0 and small-signal deviations by  $\tilde{\cdot}$ , e.g.  $\hat{\omega}_g = \hat{\omega}_{g0} + \tilde{\omega}_g$ . Accurate circuit parameter estimates and grid-voltage estimation are assumed. Hence,  $\mathbf{e}_0 = 0$ ,  $\omega_{g0} = \hat{\omega}_{g0}$ ,  $\vartheta_{g0} = \hat{\vartheta}_{g0}$ ,

and  $\hat{u}_{g0} = u_{g0}$  hold in the operation point. Then, the linearized estimation error dynamics are

$$\begin{aligned} \frac{d\tilde{\mathbf{e}}}{dt} &= (\mathbf{A}_0 - \mathbf{L}_0\mathbf{C}_c)\tilde{\mathbf{e}} + \mathbf{B}_g \underbrace{[e^{j(\tilde{\vartheta}_g - \hat{\vartheta}_g)}]}_{\approx 1 + j(\tilde{\vartheta}_g - \hat{\vartheta}_g)} (u_{g0} + \tilde{u}_g) - \hat{u}_{g0} - \tilde{u}_g \\ &= (\mathbf{A}_0 - \mathbf{L}_0\mathbf{C}_c)\tilde{\mathbf{e}} + \mathbf{B}_g[\tilde{u}_g - \hat{u}_g + j(\tilde{\vartheta}_g - \hat{\vartheta}_g)u_{g0}]. \end{aligned} \quad (5)$$

Further, if the grid voltage, the angular speed, and the angle errors are denoted by  $\tilde{u} = \tilde{u}_g - \hat{u}_g$ ,  $\tilde{\omega} = \tilde{\omega}_g - \hat{\omega}_g$ , and  $\tilde{\vartheta} = \tilde{\vartheta}_g - \hat{\vartheta}_g$ , respectively, the estimation error dynamics are

$$\frac{d}{dt} \begin{bmatrix} \tilde{\mathbf{e}} \\ \tilde{\vartheta} \end{bmatrix} = \underbrace{\begin{bmatrix} \mathbf{A}_0 - \mathbf{L}_0\mathbf{C}_c & j\mathbf{B}_g u_{g0} \\ 0 & 0 \end{bmatrix}}_{\mathbf{A}_L} \begin{bmatrix} \tilde{\mathbf{e}} \\ \tilde{\vartheta} \end{bmatrix} + \underbrace{\begin{bmatrix} \mathbf{B}_g \\ 0 \end{bmatrix}}_{\mathbf{B}_u} \tilde{u} + \underbrace{\begin{bmatrix} 0 \\ 1 \end{bmatrix}}_{\mathbf{B}_\omega} \tilde{\omega} \quad (6)$$

The converter current is the only measured state variable. Therefore, let us examine the effect of the estimation errors of the grid voltage and angular speed on the estimation error of the converter current  $\tilde{\mathbf{i}} = \tilde{\mathbf{i}}_c - \hat{\mathbf{i}}_c$ . From (6), the transfer function from the grid-voltage error to the current error is

$$\frac{\tilde{\mathbf{i}}(s)}{\tilde{u}(s)} = \tilde{\mathbf{C}}_c (s\mathbf{I} - \mathbf{A}_L)^{-1} \mathbf{B}_u = -\frac{1}{\mathbf{P}(s)} \quad (7)$$

where  $\tilde{\mathbf{C}}_c = [\mathbf{C}_c \ 0]$ , and

$$\begin{aligned} \mathbf{P}(s) &= C_f L_{fc} L_{fg} \left[ s^3 + (3j\omega_{g0} + \mathbf{l}_1) s^2 + \left( -3\omega_{g0}^2 + \frac{L_{fc} + L_{fg}}{C_f L_{fc} L_{fg}} + 2j\omega_{g0} \mathbf{l}_1 - \frac{\mathbf{l}_2}{L_{fc}} \right) s \right. \\ &\quad \left. - j\omega_{g0}^3 - \omega_{g0}^2 \mathbf{l}_1 - \frac{j\omega_{g0}}{L_{fc}} \mathbf{l}_2 \right] + j\omega_{g0} (L_{fc} + L_{fg}) + L_{fc} \mathbf{l}_1 + L_{fg} \mathbf{l}_3. \end{aligned} \quad (8)$$

Similarly, the transfer function from the angular-speed error to the current error is

$$\frac{\tilde{\mathbf{i}}(s)}{\tilde{\omega}(s)} = \tilde{\mathbf{C}}_c (s\mathbf{I} - \mathbf{A}_L)^{-1} \mathbf{B}_\omega = -\frac{j u_{g0}}{s \cdot \mathbf{P}(s)} \quad (9)$$

and the transfer function from the angle error to the current error is obtained from (9) using the relationship  $\vartheta_g = \int \omega_g dt$ , leading to  $\tilde{\vartheta} = \tilde{\omega}/s$ . It is to be noted that the observer gains ( $\mathbf{l}_1$ ,  $\mathbf{l}_2$ , and  $\mathbf{l}_3$ ) strongly affect the characteristic polynomial of the transfer functions. Further, this is seen in the orientation of the current error  $\tilde{\mathbf{i}}$  in the complex plane.

### 3.2. Selection of the Full-Order Observer Gains

The direct pole placement is a straightforward method for the selection of the full-order observer gains. This can be done assuming first the perfect grid-voltage orientation and known or measured grid voltage. Then, the characteristic polynomial of the estimator error dynamics (4) is set to correspond the third-order dynamics as follows

$$\det(s\mathbf{I} - \mathbf{A} + \mathbf{L}\mathbf{C}_c) = (s + \alpha_{o1})(s^2 + 2\zeta_{o2}\omega_{o2}s + \omega_{o2}^2), \quad (10)$$

where  $\alpha_{o1}$  determines the first-order pole and  $\zeta_{o2}$  and  $\omega_{o2}$  the second-order pole pair of the estimator dynamics. This gives the gains

$$\mathbf{l}_1 = \alpha_{o1} + 2\zeta_{o2}\omega_{o2} - 3j\omega_{g0} \quad (11a)$$

$$\mathbf{l}_2 = -L_{fc} \left( 2\alpha_{o1}\zeta_{o2}\omega_{o2} + \omega_{o2}^2 + 3\omega_{g0}^2 - \frac{L_{fc} + L_{fg}}{L_{fc} L_{fg} C_f} - 2j\omega_{g0} \mathbf{l}_1 \right) \quad (11b)$$

$$\mathbf{l}_3 = \alpha_{o1}\omega_{o2}^2 C_f L_{fc} + j\omega_{g0} \left( \omega_{g0}^2 C_f L_{fc} - \frac{L_{fc}}{L_{fg}} - 1 \right) + \left( \omega_{g0}^2 C_f L_{fc} - \frac{L_{fc}}{L_{fg}} \right) \mathbf{l}_1 + j\omega_{g0} C_f \mathbf{l}_2. \quad (11c)$$

The observer gains are functions of the system parameters, the grid angular frequency at the operating point and the desired poles of the estimation error dynamics. The poles can be seen as tuning parameters and their selection can be based on the open-loop system, as described in [15].

### 3.3. Adaptation Laws

Since the grid voltage is not measured, the observer in (3) is supplemented with the adaptation of the magnitude and angle of the grid voltage. Here, quasi-steady-state analysis is used to design the adaptation loops. The estimation error dynamics of the full-order observer in (6) are considered to be much faster than the adaptation mechanisms of the grid voltage and its angle. The different time scales enable considering the current estimation error  $\tilde{\mathbf{i}} = \tilde{\mathbf{i}}_c - \hat{\mathbf{i}}_c$  being in steady state from the viewpoint of the adaptation. If the gains (11) are inserted in (7), the transfer function reduces to

$$\mathbf{G}_{iu}(s) = \frac{\tilde{\mathbf{i}}(s)}{\tilde{u}(s)} = -\frac{1}{C_f L_{fc} L_{fg} (s + \alpha_{o1}) (s^2 + 2\zeta_{o2} \omega_{o2} s + \omega_{o2}^2)} \quad (12)$$

Similarly, if the gains (11) are inserted in (9), the transfer function becomes

$$\mathbf{G}_{i\omega}(s) = \frac{\tilde{\mathbf{i}}(s)}{\tilde{\omega}(s)} = -\frac{j u_{g0}}{s \cdot C_f L_{fc} L_{fg} (s + \alpha_{o1}) (s^2 + 2\zeta_{o2} \omega_{o2} s + \omega_{o2}^2)} \quad (13)$$

Assuming these transfer functions to be in steady state (i.e.,  $s = 0$ ) leads to

$$\tilde{\mathbf{i}} = -\frac{1}{C_f L_{fc} L_{fg} \alpha_{o1} \omega_{o2}^2} \tilde{u} - j \frac{u_{g0}}{C_f L_{fc} L_{fg} \alpha_{o1} \omega_{o2}^2} \tilde{\vartheta}. \quad (14)$$

This equation shows that the d component  $\tilde{i}_d$  of the estimation error is affected by the grid-voltage estimation error  $\tilde{u}$  and the q component  $\tilde{i}_q$  is affected by the angle error ( $\tilde{\vartheta} = \tilde{\omega}/s$ ). These observations point out that the estimation of the grid voltage and its angular speed can be based on regulating the error between the converter current and estimated current to be zero. Hence, the adaptation laws for the grid voltage and its angular speed can be constructed as follows

$$\hat{u}_g = k_{pu} \tilde{i}_d + k_{iu} \int \tilde{i}_d dt, \quad \hat{\omega}_g = k_{p\omega} \tilde{i}_q + k_{i\omega} \int \tilde{i}_q dt \quad (15)$$

where  $k_{pu}$ ,  $k_{iu}$ ,  $k_{p\omega}$ , and  $k_{i\omega}$  are the gains of the adaptation-loop controllers.

It is worth noting that the selection of the observer gains has significant effect on the formulation of the adaptation laws. If zero observer gains are inserted in (7) and (9), the current components for the adaptation loops should be selected opposite. This can be easily shown with a similar quasi-steady-state analysis, which gives

$$\tilde{\mathbf{i}} = -\frac{u_{g0}}{\omega_{g0} (L_{fc} + L_{fg} - \omega_{g0}^2 C_f L_{fc} L_{fg})} \tilde{\vartheta} + j \frac{1}{\omega_{g0} (L_{fc} + L_{fg} - \omega_{g0}^2 C_f L_{fc} L_{fg})} \tilde{u} \quad (16)$$

in the case of zero observer gains. The d component  $\tilde{i}_d$  of the converter current error is affected by the angle error  $\tilde{\vartheta}$  and the q component  $\tilde{i}_q$  by the voltage error, which is opposite to (14).

### 3.4. Adaptation-Loop Gains

Figs. 3(a) and 3(b) show the linearized adaptation loops of the grid voltage and its angular speed. The gains of the adaptation-loop controllers can be selected to give the approximate bandwidth of  $\alpha_u$  for the estimation dynamics of the amplitude of the grid voltage and the natural frequency of  $\omega_\omega$  for the estimation dynamics of the angular frequency of the grid voltage. Considering the estimation error of the converter current in steady state as in (14) and selecting

$$k_{pu} = 0 \quad \text{and} \quad k_{iu} = -\alpha_u \cdot C_f L_{fc} L_{fg} \alpha_{o1} \omega_{o2}^2, \quad (17)$$

in (15), the closed-loop transfer function of the linearized grid-voltage adaptation loop is

$$G_u(s) = \frac{\tilde{u}_g(s)}{\tilde{u}(s)} = \frac{\alpha_u}{s + \alpha_u} \quad (18)$$

with the bandwidth of  $\alpha_u$ . Similarly, using the steady-state approximation (14), the gains for the adaptation law of the angular speed in (15) can be selected as

$$k_{pw} = -2\zeta_\omega\omega_\omega \cdot C_f L_{fc} L_{fg} \alpha_{o1} \omega_{o2}^2 / u_{g0} \quad \text{and} \quad k_{i\omega} = -\omega_\omega^2 \cdot C_f L_{fc} L_{fg} \alpha_{o1} \omega_{o2}^2 / u_{g0}. \quad (19)$$

Then, the closed-loop transfer function of the approximated and linearized adaptation loop of the angular speed is

$$G_\omega(s) = \frac{\tilde{\omega}_g(s)}{\tilde{\omega}_\omega(s)} = \frac{2\zeta_\omega\omega_\omega s + \omega_\omega^2}{s^2 + 2\zeta_\omega\omega_\omega s + \omega_\omega^2} \quad (20)$$

with the natural frequency of  $\omega_\omega$  and damping of  $\zeta_\omega$ .

### 3.5. Small-Signal Stability

The quasi-steady-state approximations can be used to give simple tuning for adaptation loops. However, if the bandwidths of the adaptation loops are increased close to the bandwidth of the full-order observer, the quasi-steady-state assumption is not valid anymore and the stability of the loops can be lost. In the following, the small-signal stability of the adaptation loops is analyzed.

With the selected tuning, the closed-loop transfer function of the adaptation loop of the grid voltage magnitude is

$$\begin{aligned} G_u(s) &= \frac{\text{Re}\{\mathbf{G}_{iu}(s)\} \left(k_{pu} + \frac{k_{iu}}{s}\right)}{1 + \text{Re}\{\mathbf{G}_{iu}(s)\} \left(k_{pu} + \frac{k_{iu}}{s}\right)} = \frac{k_{iu}}{s / \text{Re}\{\mathbf{G}_{iu}(s)\} + k_{iu}} \\ &= \frac{\alpha_u \cdot \alpha_{o1} \omega_{o2}^2}{s^4 + (\alpha_{o1} + 2\zeta_{o2} \omega_{o2}) s^3 + (2\alpha_{o1} \zeta_{o2} \omega_{o2} + \omega_{o2}^2) s^2 + \alpha_{o1} \omega_{o2}^2 s + \alpha_u \cdot \alpha_{o1} \omega_{o2}^2}. \end{aligned} \quad (21)$$

Since the degree of characteristic polynomial is four, analytical calculation of the poles becomes difficult. However, the stability can be tested using the Routh-Hurwitz stability criterion [16]. This gives necessary and sufficient conditions for the stability of the system. As an example, the polynomial  $P(s) = a_4 s^4 + a_3 s^3 + a_2 s^2 + a_1 s + a_0$ , has the roots with negative real parts and is thus stable (Hurwitz polynomial), if the following conditions are fulfilled:  $a_i > 0$  for all  $i = 0 \dots 4$ ,  $a_2 a_3 > a_1 a_4$ , and  $a_1 a_2 a_3 > a_0 a_3^2 + a_1^2 a_4$ .

According to polynomial of the example, the stability criterion for the magnitude adaptation is: all the tuning parameters  $\alpha_{o1}$ ,  $\omega_{o2}$ ,  $\zeta_{o2}$ , and  $\alpha_u$  (i.e., desired poles of the observer and the adaptation loop) must be positive and it is necessary that

$$\alpha_u < (a_2 a_3 - a_1) / a_3^2, \quad (22)$$

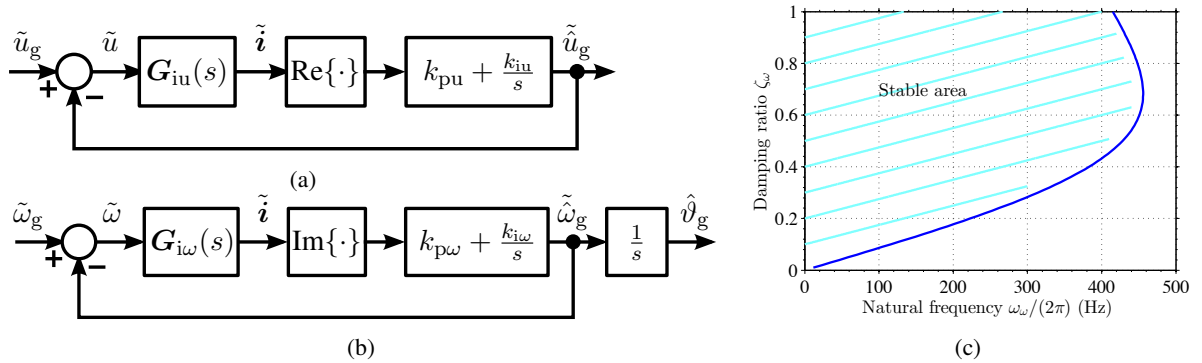


Fig. 3: (a) Block diagram of the linearized adaptation loop of grid voltage estimation; (b) Block diagram of the linearized adaptation loop of the grid angle estimation. The transfer functions  $G_{iu}(s)$  and  $G_{i\omega}(s)$  are obtained from (6); (c) Region of the stable operation of the angle adaptation loop when the tuning of the full-order observer is:  $\alpha_{o1} = 2\pi \cdot 1000$  rad/s,  $\omega_{o2} = 2\pi \cdot 1420$  rad/s, and  $\zeta_{o2} = 0.5$ . With the selected tuning, the stable area is limited by the boundary condition of (25).

where  $a_3 = \alpha_{o1} + 2\zeta_{o2}\omega_{o2}$ ,  $a_2 = 2\alpha_{o1}\zeta_{o2}\omega_{o2} + \omega_{o2}^2$  and  $a_1 = \alpha_{o1}\omega_{o2}^2$ . The equation determines the upper limit for the tuning parameter  $\alpha_u$ , which is the approximate bandwidth for the estimation of the grid-voltage magnitude. As an example, if  $\alpha_{o1} = 2\pi \cdot 1000$  rad/s,  $\omega_{o2} = 2\pi \cdot 1420$  rad/s and  $\zeta_{o2} = 0.5$  are selected, the condition  $\alpha_u < 2\pi \cdot 1075$  rad/s must hold.

When the selected tuning is used, the closed-loop transfer function of the angle adaptation loop is

$$G_\omega(s) = \frac{\text{Im}\{\mathbf{G}_{i\omega}(s)\} \left(k_{p\omega} + \frac{k_{i\omega}}{s}\right)}{1 + \text{Im}\{\mathbf{G}_{i\omega}(s)\} \left(k_{p\omega} + \frac{k_{i\omega}}{s}\right)} \quad (23)$$

$$= \frac{2\zeta_\omega\omega_\omega \cdot \alpha_{o1}\omega_{o2}^2s + \omega_\omega^2 \cdot \alpha_{o1}\omega_{o2}^2}{s^2 \cdot (s + \alpha_{o1})(s^2 + 2\zeta_{o2}\omega_{o2}s + \omega_{o2}^2) + 2\zeta_\omega\omega_\omega \cdot \alpha_{o1}\omega_{o2}^2s + \omega_\omega^2 \cdot \alpha_{o1}\omega_{o2}^2}$$

The Routh-Hurwitz stability criterion for this system is: all the tuning parameters  $\alpha_{o1}$ ,  $\omega_{o2}$ ,  $\zeta_{o2}$ ,  $\omega_\omega$ , and  $\zeta_\omega$  must be positive and it is necessary that

$$\omega_\omega^2 - 2e \cdot \zeta_\omega\omega_\omega + \frac{f}{e} > 0 \quad (24)$$

and

$$-\omega_\omega^3 + 4e \cdot \zeta_\omega\omega_\omega^2 - \omega_\omega \left(\frac{f^2}{\alpha_{o1}\omega_{o2}^2 \cdot e} + 4\zeta_\omega^2 \cdot e^2 + \frac{f}{e}\right) + 2\zeta_\omega \cdot f > 0, \quad (25)$$

where  $e = \alpha_{o1} + 2\zeta_{o2}\omega_{o2}$  and  $f = 2\zeta_{o2}\omega_{o2}(\omega_{o2}^2 + \alpha_{o1}^2 + 2\alpha_{o1}\zeta_{o2}\omega_{o2})$ . The boundary condition of the equation (25) is illustrated in Fig. 3(c). It is to be noted that the derived stability conditions determine the local stability of the nonlinear estimation error dynamics in ideal conditions. In the true system, errors due to the discretization and parameter uncertainties naturally shrink the stable operation area. However, the presented conditions can be seen as an uppermost limits for the design and they can be used to perceive the limitations of the tuning.

## 4. Control System

The block diagram of the control system comprising cascaded DC-voltage and current control loops is shown in Fig. 2. State-space current control [15] is implemented in the estimated grid-voltage reference frame. The current controller and the observer are discretized using Tustin's method. The PI regulators of the adaptation loops and DC-voltage control are discretized using the forward Euler method. The components of the current reference  $\mathbf{i}_{c,\text{ref}} = i_{cd,\text{ref}} + j i_{cq,\text{ref}}$  are calculated in the steady state. From (2), the grid current is  $\mathbf{i}_g = (\mathbf{i}_c - j\hat{\omega}_g C_f \mathbf{u}_g)/(1 - \hat{\omega}_g^2 C_f L_{fg})$ . The complex power at the point of common coupling is  $s_g = 3/2 \cdot \mathbf{u}_g \mathbf{i}_g^* = p_g + j q_g$ . Assuming  $\mathbf{i}_c = \mathbf{i}_{c,\text{ref}}$ , the current references become

$$i_{cd,\text{ref}} = \frac{2}{3} \frac{1 - \hat{\omega}_g^2 C_f L_{fg}}{\hat{u}_g} p_{\text{ref}}, \quad i_{cq,\text{ref}} = -\frac{2}{3} \frac{1 - \hat{\omega}_g^2 C_f L_{fg}}{\hat{u}_g} q_{\text{ref}} + \hat{\omega}_g C_f \hat{u}_g, \quad (26)$$

where the peak-value scaling of the space vectors is used, and  $p_{\text{ref}}$  and  $q_{\text{ref}}$  are the references for the active and reactive power, respectively. The active power reference is the output of DC-voltage control, which is implemented indirectly by means of DC-capacitor energy control [17, 18]. A pure PI-controller is used for the capacitor energy control, as in [17], but the tuning is based on the parameters of the system, as in [18]. The space-vector pulse-width modulation (SVPWM) is used and a simple current feedforward dead-time compensation is added [19]. The effect of the delay on the synchronous-to-stationary reference frame transformation is compensated for by modifying the transformation  $e^{j\hat{\theta}_g} \rightarrow e^{j(\hat{\theta}_g + \vartheta_d)}$ , where  $\vartheta_d = (3/2) \cdot \hat{\omega}_g T_s$  as described in [20].

It is worth noticing that the tuning of the control system can be automated, if the equivalent circuit parameters of the system are known or estimated. All the observer gains (11), (17), and (19) are functions



Table I: System parameters.

Parameter	Value	Parameter	Value
$u_g$	$\sqrt{2/3} \cdot 400$ V (1 p.u.)	$\omega_g$	$2\pi \cdot 50$ rad/s
$i_N$	$\sqrt{2} \cdot 18$ A (1 p.u.)	$C_f$	$10 \mu\text{F}$ (0.040 p.u.)
$L_{fc}$	2.94 mH (0.072 p.u.)	$L_{fg}$	1.96 mH (0.048 p.u.)
$f_{sw}$	6 kHz	$T_s$	$1/(2f_{sw})$

of the equivalent circuit parameters and desired dynamic performance specifications. Either nominal or estimated values could be used for the operation-point grid voltage in the gain expressions (nominal values are used in this paper). As the input values for the tuning, the dynamic performance specifications must be determined: 1) desired bandwidth and the resonance damping of the LCL filter for the state-space controller, 2) convergence dynamics of the estimation error for the full-order observer, 3) approximate bandwidths for the controllers in the adaptation loops. The robustness of the control system depends on the selected performance specifications. The more robust system is desired, the slower dynamic performance should be specified.

In this paper, the following performance specifications are used. The current controller is tuned to give an approximate bandwidth of  $2\pi \cdot 500$  rad/s as in [15]. The dominant dynamics of the observer is set twice as fast as the current control, i.e.,  $\alpha_{o1} = 2\pi \cdot 1000$  rad/s and the second-order pole of the observer  $\omega_{o2}$  is set to correspond to the resonance frequency  $\omega_p^s = 2\pi \cdot 1470$  rad/s of the LCL filter in the synchronous reference frame, i.e.,  $\omega_{o2} = \omega_p^s - \omega_g$ . The damping of this pole pair is set to  $\zeta_{o2} = 0.5$ . The tuning of the adaptation loops is set, with a good damping, approximately one decade below the theoretical limits obtained from (22), (24) and (25). Thus, the tuning parameters for the adaptation loops are:  $\alpha_u = 2\pi \cdot 100$  rad/s,  $\omega_\omega = 2\pi \cdot 50$  rad/s and  $\zeta_\omega = 0.9$ . The DC-voltage regulator bandwidth [18] is set approximately one decade below the current controller bandwidth. The system parameters are given in Table I.

## 5. Experimental Results

The proposed grid-voltage sensorless scheme was experimentally tested using a 12.5-kVA, 400-V, grid-connected converter equipped with an LCL filter. The control of the converter was implemented on dSPACE DS1006, DS2201, and DS5202 boards. The switching frequency of the converter was  $f_{sw} = 6$  kHz, and synchronous sampling, twice per carrier, was used. The DC-link voltage was regulated to 650 V and the converter under test was loaded with another back-to-back connected converter (12.5 kVA, 400 V) with an LCL filter. An isolation transformer was used in the grid connection of the loading converter.

Fig. 4(a) illustrates the operation of the converter when an impulse disturbance of  $-60^\circ$  was applied into the estimated grid-voltage angle  $\hat{\vartheta}_g$  inside the control system. The converter was supplying a power of

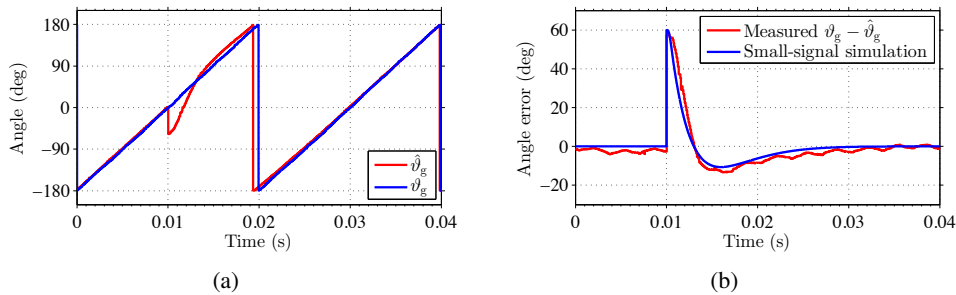


Fig. 4: Experimental results when a step disturbance in the angle estimate of the grid voltage is applied: (a) estimated and measured angles,  $\hat{\vartheta}_g$  and  $\vartheta_g$ , respectively; (b) simulated and measured angle errors.

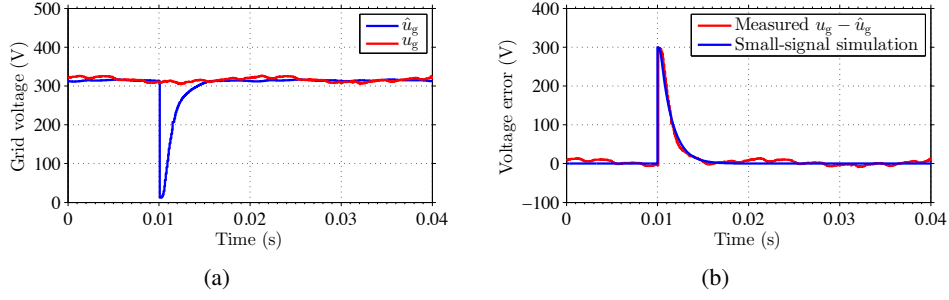


Fig. 5: Experimental results when a step disturbance in the amplitude estimate of the grid voltage is applied: (a) estimated and measured amplitudes of the grid voltage; (b) simulated and measured amplitude errors.

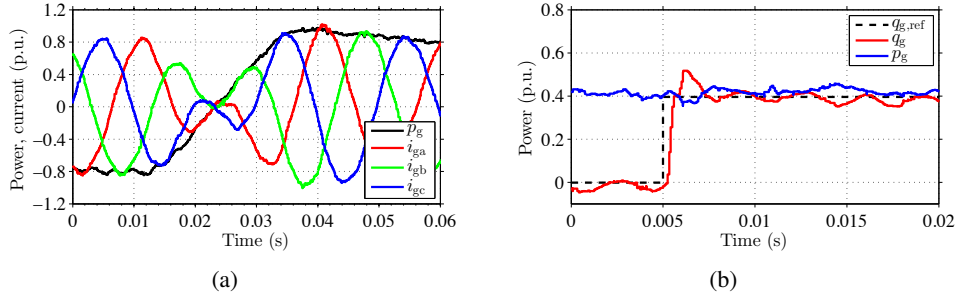


Fig. 6: Experimental results: (a) Operation with both power directions. Phase currents and the power  $p_g$  are measured from the grid-side of the LCL filter; (b) Waveforms of the active power  $p_g$  and reactive power  $q_g$  injected to the grid at the grid-side of the LCL filter, when a step of 5 kvar (0.4 p.u.) is applied into the reactive power reference  $q_{g,ref}$ . A 20-ms period is shown.

5 kW (0.4 p.u.) to the grid. Fig. 4(b) compares the measured and simulated waveforms of the estimated grid-voltage angle error during the disturbance. In the simulation, an angular speed impulse corresponding a disturbance of  $-60^\circ$  in the angle estimate was applied in  $\tilde{\omega}_g$  in the small-signal model shown in Fig. 3(b). As can be seen from the Fig. 4(b), the agreement with the small-signal simulation and the measurement is good.

Measured dynamic behavior of the estimation of the grid voltage amplitude is shown in Fig. 5(a), when a disturbance of  $-300$  V was applied in the amplitude estimate. The converter was supplying the power of 5 kW. Experimental results are compared with the small-signal simulations in Fig. 5(b). In the simulations, step of 300 V was applied in the signal  $\tilde{u}_g$  in the small-signal model shown in Fig. 3(a). The results of Fig. 5(b) indicate good agreement with the small-signal simulation and the measurement.

Fig. 6(a) demonstrates the ability to operate with both power directions. The loading condition of the converter under test was changed from  $-10$  kW to 10 kW by changing the direction of the active power of the load connected to the DC bus. Further, dynamic performance of the current control is illustrated in Fig. 6(b), when a step of 5 kvar was applied into the reference of the reactive power  $q_g$ . At the same time, the converter was supplying the active power of  $p_g \approx 5$  kW. As Fig. 6(b) shows, the resonance of the LCL filter is effectively damped and the reactive power rapidly follows its reference according to the designed dynamics of the current control.

## 6. Conclusions

This paper presents an adaptive full-order observer for the grid-voltage sensorless control of a grid-connected converter equipped with an LCL filter. Converter-side currents of the LCL filter and DC voltage are only measured variables, and the full-order observer is used for state estimation. Further, the magnitude and angle of the grid voltage are estimated using the converter current estimation error as an

input for adaptation loops. Presented analytical design of the adaptation loops gives simple expressions for the observer and adaptation gains, which enables automatic tuning. Experimental results indicate fast tracking of the magnitude and angle of the grid voltage. The proposed estimation scheme is a sensorless alternative to conventional PLLs and it could be applied, e.g., in the grid-connected converter of a motor drive. Reduced number of sensors provides cost advantages and decreases amount of sensor wiring.

## References

- [1] I. Agirman and V. Blasko, "A novel control method of a VSC without AC line voltage sensors," *IEEE Trans. Ind. Appl.*, vol. 39, no. 2, pp. 519–524, Mar./Apr. 2003.
- [2] T. Ohnishi and K. Fujii, "Line voltage sensorless three phase PWM converter by tracking control of operating frequency," in *Proceedings of the Power Conversion Conference - Nagaoka 1997*, vol. 1, Nagaoka, Japan, 1997, pp. 247–252.
- [3] T. Noguchi, H. Tomiki, S. Kondo, and I. Takahashi, "Direct power control of PWM converter without power-source voltage sensors," *IEEE Trans. Ind. Appl.*, vol. 34, no. 3, pp. 473–479, May/June. 1998.
- [4] M. Malinowski, M. P. Kazmierkowski, S. Hansen, F. Blaabjerg, and G. D. Marques, "Virtual-flux-based direct power control of three-phase PWM rectifiers," *IEEE Trans. Ind. Appl.*, vol. 37, no. 4, pp. 1019–1027, Jul./Aug. 2001.
- [5] J. A. Suul, A. Luna, P. Rodriguez, and T. Undeland, "Voltage-sensor-less synchronization to unbalanced grids by frequency-adaptive virtual flux estimation," *IEEE Trans. Ind. Electron.*, vol. 59, no. 7, pp. 2910–2923, Jul. 2012.
- [6] H.-S. Song, I.-W. Joo, and K. Nam, "Source voltage sensorless estimation scheme for PWM rectifiers under unbalanced conditions," *IEEE Trans. Ind. Electron.*, vol. 50, no. 6, pp. 1238–1245, Dec. 2003.
- [7] A. E. Leon, J. A. Solsona, and M. I. Valla, "Control strategy for hardware simplification of voltage source converter-based power applications," *IET Power Electronics*, vol. 4, no. 1, pp. 39–50, Jan. 2011.
- [8] D.-C. Lee and D.-S. Lim, "AC voltage and current sensorless control of three-phase PWM rectifiers," *IEEE Trans. Power Electron.*, vol. 17, no. 6, pp. 883–890, Nov. 2002.
- [9] B. Bolsens, K. De Brabandere, J. Van den Keybus, J. Driesen, and R. Belmans, "Model-based generation of low distortion currents in grid-coupled PWM-inverters using an LCL output filter," *IEEE Trans. Power Electron.*, vol. 21, no. 4, pp. 1032–1040, Jul. 2006.
- [10] S. Mariéthoz and M. Morari, "Explicit model-predictive control of a PWM inverter with an LCL filter," *IEEE Trans. Ind. Electron.*, vol. 56, no. 2, pp. 389–399, Feb. 2009.
- [11] M. Malinowski and S. Bernet, "A simple voltage sensorless active damping scheme for three-phase PWM converters with an LCL filter," *IEEE Trans. Ind. Electron.*, vol. 55, no. 4, pp. 1876–1880, Apr. 2008.
- [12] K. H. Ahmed, A. M. Massoud, S. J. Finney, and B. W. Williams, "Sensorless current control of three-phase inverter-based distributed generation," *IEEE Trans. Power Del.*, vol. 24, no. 2, pp. 919–929, Apr. 2009.
- [13] Y. A.-R. I. Mohamed, M. A-Rahman, and R. Seethapathy, "Robust line-voltage sensorless control and synchronization of LCL-filtered distributed generation inverters for high power quality grid connection," *IEEE Trans. Power Electron.*, vol. 27, no. 1, pp. 87–98, Jan. 2012.
- [14] Y. A.-R. I. Mohamed and E. F. El-Saadany, "Adaptive discrete-time grid-voltage sensorless interfacing scheme for grid-connected DG-inverters based on neural-network identification and deadbeat current regulation," *IEEE Trans. Power Electron.*, vol. 23, no. 1, pp. 308–321, Jan. 2008.
- [15] J. Kukkola and M. Hinkkanen, "Observer-based state-space current control for a three-phase grid-connected converter equipped with an LCL filter," *IEEE Trans. Ind. Appl.*, vol. 50, no. 4, Jul./Aug. 2014.
- [16] G. F. Franklin, J. D. Powell, and A. Emami-Naeini, *Feedback Control of Dynamic Systems*. New Jersey: Prentice-Hall, 2002.
- [17] N. Hur, J. Jung, and K. Nam, "A fast dynamic DC-link power-balancing scheme for a PWM converter-inverter system," *IEEE Trans. Ind. Electron.*, vol. 48, no. 4, pp. 794–803, Aug. 2001.
- [18] R. Ottersten, "On control of back-to-back converters and sensorless induction machine drives," Ph.D. dissertation, Dept. Elect. Power Eng., Chalmers Univ. of Technol., Göteborg, Sweden, 2003.
- [19] J. K. Pedersen, F. Blaabjerg, J. W. Jensen, and P. Thogersen, "An ideal PWM-VSI inverter with feedforward and feedback compensation," in *Fifth European Conference on Power Electronics and Applications (EPE 1993)*, vol. 5, Brighton, U.K, Sep. 1993, pp. 501–507.
- [20] B.-H. Bae and S.-K. Sul, "A compensation method for time delay of full-digital synchronous frame current regulator of PWM AC drives," *IEEE Trans. Ind. Appl.*, vol. 39, no. 3, pp. 802–810, May/June. 2003.